Journal of Biomechanics 131 (2022) 110868

Contents lists available at ScienceDirect

Journal of Biomechanics

journal homepage: www.elsevier.com/locate/jbiomech

A simplified homogenization model applied to viscoelastic behavior of cortical bone at ultrasonic frequencies

Reidmen Aróstica [a], Ana Aguilera [d], Axel Osses [a,b,c], Jean-Gabriel Minonzio [d,e,*]

[a] Departamento de Ingeniería Matemática and Center for Mathematical Modeling UMI CNRS 2807, FCFM, Universidad de Chile, Av. Beaucheff 851, Santiago, Chile
[b] Millenium Nucleus in Cardiovascular Magnetic Resonance, Cardio MR, Chile
[c] Millenium Nucleus Applied Control and Inverse Problems, ACIP, Chile
[d] Escuela de Ingeniería Informática, Universidad de Valparaíso, Valparaíso, Chile
[e] Centro de Investigación y Desarrollo en Ingeniería en Salud, Universidad de Valparaíso, Valparaíso, Chile

ARTICLE INFO

Keywords:
Cortical bone
Homogenization theory
Viscoelasticity
Microstructure mechanics
Multiscale
Quality factor
Attenuation
Ultrasound

ABSTRACT

Cortical bone is a complex multiscale medium and its study is of importance for clinical fracture prevention. In particular, cortical attenuation is known to be linked with shock energy absorption and ability to resist fracture. However, the links between cortical bone absorption and its multiscale structure are still not well understood. This work is about the use of homogenized tensors in order to characterize the viscoelastic behavior of cortical bone at ultrasonic frequencies, i.e., about 0.1 to 10 MHz. Such tensors are derived from the cell problem via two-scale homogenization theory for linear elastic and Kelvin–Voigt viscoelastic descriptions. The elliptic formulations obtained from the cell problems are implemented within the range of medically-observed porosities. Microstructure is assessed considering cubic cells with cylindrical inclusion and transverse isotropic assumption. A simplified model, adding one temporal parameter τ per phase, allows a good agreement with experimental data. The corresponding attenuation is proportional to the square of the frequency, in agreement with Kramer–Kronig relations. This development is proposed in the context of robust clinical inverse problem approaches using a restricted number of parameter. Two main properties for the material filling the pores are adjusted and discussed: absorption and shear contribution. Best agreement with experimental data is observed for material inside the pores being solid and highly attenuating.

1. Introduction

Complex multiscale problems are often encountered in Biology or Medicine. One particular example is cortical bone, which study is of importance for fracture prevention. Cortical bone is a composite structure with two main phases: a solid part, denoted bone matrix or extra vascular matrix (EVM), and a porous part containing biological fluids, such as blood and marrow (Milovanovic et al., 2017). The solid part is organized at different scales from the nanometric fundamental elements, i.e., type I collagen stiffened by crystals of calcium hydroxyapatite (Groetsch et al., 2019) through a micrometer scale, i.e., lamellae (about 10 μm) (Granke et al., 2013) until sub millimeter scale, i.e. osteon (about 0.3 mm). The latter is also known as the fundamental functional unit of cortical bone. Similarly, the porous network is also multiscale organized, from the canaliculi (about 1 μm), the lacunae containing osteocytes and (about 10 μm) to the Volkman's and Havers' canals, with typical sizes of about 10 and 50 μm, respectively (Núñez et al., 2017). Moreover, unbalanced bone remodeling tends to induce resorption cavities ranging from 50 to 200 μm. Finally, cortical bone thickness, embedding both solid and fluid phases, typically ranges from 1 to 6 mm (Karjalainen et al., 2008).

The lower scales have been mainly explored on *ex vivo* samples using different techniques (Akhter and Recker, 2021) such as nano indentation (Vennin et al., 2017), synchrotron micro Computed Tomography (μCT) (Groetsch et al., 2019), Scanning Acoustic Microscopy (SAM) (Iori et al., 2020). *In vivo* measurements, such as Quantitative CT (QCT) (Ahmed et al., 2015), High Resolution-pQCT (HR-pQCT) (Sundh et al., 2017), Magnetic Resonance Imaging (MRI) (Hong et al., 2019), up to 1 MHz Ultrasound (Minonzio et al., 2019) mainly focus on the mesoscale. Indeed, with typical millimeter resolutions, cortical bone is thus clinically explored as a homogeneous medium allowing to provide cortical porosity estimates or index, being potential clinical parameters (Bjørnerem, 2016). Note that recent development aims to explore

* Corresponding author at: Escuela de Ingeniería Informática, Universidad de Valparaíso, Valparaíso, Chile.
E-mail addresses: reidmen@dim.uchile.cl (R. Aróstica), ana.aguilera@uv.cl (A. Aguilera), axosess@dim.uchile.cl (A. Osses), jean-gabriel.minonzio@uv.cl (J.-G. Minonzio).

https://doi.org/10.1016/j.jbiomech.2021.110868
Accepted 16 November 2021
Available online 30 November 2021

cortical at a lower scale, such HR-pQCT second generation (Hildebrand et al., 2021) or higher frequency Ultrasound (Yousefian et al., 2021; Ishimoto et al., 2019).

As for elasticity, viscoelasticity can be experimentally assessed on *ex vivo* specimen at lower scale using nanoindentation (Fan and Rho, 2003; Wu et al., 2012) or at the mesoscale using dynamic mechanical testing (Iyo et al., 2004; Yamashita et al., 2001) or ultrasound using different methods such as transmission (Sasso et al., 2008) and Resonant Spectroscopy Ultrasound (RUS) (Bernard et al., 2016). *In vivo* measurement of attenuation has been recently proposed using audible (Aygün, 2019) or ultrasonic (Minonzio et al., 2021) frequencies.

Improving multiscale modeling of cortical bone has already been explored , with homogenization approaches similar to those applied to composites (Penta and Gerisch, 2015) or poroelastic (Dehghani et al., 2018). In 2009, an asymptotic homogenization model was proposed for cortical bone, in order to interpret the overall elasticity in function of the mesoscale porosity, i.e., Haversian canals and resorption cavities (Parnell and Grimal, 2009). Authors considered an isotropic bone matrix and used an approximated solution of the cell problem proposed in a previous study (Parnell and Abrahams, 2008). The asymptotic homogenization model was then improved by taking into account a transverse anisotropy for the bone matrix (Parnell et al., 2012). In the same paper, authors used the Mori–Tanaka scheme and the Hashin–Rosen bounds. Other approaches have completed the asymptotic homogenization, such as micromechanical modeling (Salguero et al., 2014), stochastic homogenization (Gagliardi et al., 2018), three scales asymptotic homogenization (Ramírez-Torres et al., 2018). The influence of the fluid presence inside the pores has also been recently studied (Nguyen et al., 2018; Zhou et al., 2020). Viscoelasticity has been introduced in homogenization models in a few studies about composites (Yi et al., 1998; Abdessamad et al., 2009; Cruz González et al., 2020) or cortical bone (Nguyen et al., 2018).

The aim of this paper is to propose a simplified model to interpret ultrasonic measurements of cortical bone viscoelastic behavior. This approach is derived from an asymptotic two-scale homogenization model taking into account Kelvin–Voigt viscoelasticity at both scales (Panasenko, 2005). This development is proposed in the context of robust clinical inverse problem approaches using a restricted number of parameters (Minonzio et al., 2019). The paper is organized as follows: in Section 2, modeling assumptions and theoretical description are presented In Section 3, different sets of parameters are tested compared to experimental data. Finally in Section 4, the predictions obtained and their implications are discussed and compared with the state of the art.

2. Theoretical description

Following the biomedical literature (Parnell and Grimal, 2009; Parnell et al., 2012; Cai et al., 2019), we assume from a mechanical point of view the cortical bone mesoscale as a two-phase composite material, described by a soft phase formed mainly of pores containing organic fluids embedded in a hard matrix phase of hydroxyapatite and collagen fibers. Mesoscale porosities are characterized by two main structures: the resorption cavities (size of approx. 50–200 [μm]) and haversian canals (with size approx. 50 [μm]) mainly distributed along the long axis of bone and periodically over the radial axis. Such distribution enables us to describe the composite material on macro- and microscopic structures denoting such systems by the variables $\mathbf{x} = [x_1, x_2, x_3]$ and $\mathbf{y} = [y_1, y_2, y_3]$ respectively, being related by $\mathbf{y} = \mathbf{x}/\epsilon$ with $\epsilon > 0$ the ratio of high oscillation for the bone associated to its microstructure dimensions (approx. 50 [μm]). Schematically, Fig. 1 describes our idealized composed material under study. The 3D-periodic cell is a fluid filled cylinder included in a unitary cube.

2.1. Elastic model

As first approximation, we assume a multiscale mechanical behavior of cortical bone of linear type, i.e., characterized by a linear elastic tensor $\mathbf{C}(\mathbf{x}) = (C_{ijkl}(\mathbf{x}))_{ijkl}$, a mass density ρ and a scale parameter $\epsilon > 0$ fixed. We assume the domain of interest denoted by $\Omega \subset \mathbb{R}^3$, with characteristic microstructure $\mathbf{Y} \subset \mathbb{R}^3$ described by the displacement solution $u^\epsilon(\mathbf{x}, t)$ satisfying the system:

$$\begin{aligned} \rho^\epsilon(\mathbf{x})\partial_{tt}u^\epsilon(\mathbf{x},t) - \nabla\cdot\sigma^\epsilon(\mathbf{x},t) &= \mathbf{f}(\mathbf{x},t) \quad \text{in} \quad \Omega\times(0,T) \\ \sigma^\epsilon_{ij}(\mathbf{x},t) &= C^\epsilon_{ijkl}(\mathbf{x})\mathbf{e}_{kl}(u^\epsilon(\mathbf{x},t)) \quad \text{in} \quad \Omega\times(0,T), \end{aligned} \tag{1}$$

where we use the notation $C^\epsilon_{ijkl}(\mathbf{x}) = C_{ijkl}(\mathbf{x}/\epsilon)$ for the elastic periodic tensor and $\mathbf{e}_{kl}$ as the symmetric gradient. Here, $\rho^\epsilon(\mathbf{x}) = \rho(\frac{\mathbf{x}}{\epsilon})$ is the periodic material density and $\mathbf{f}(\mathbf{x}, t)$ are macroscopic external forces. We also assume homogeneous Dirichlet and Neumann boundary conditions on the subregions Γ_N and Γ_D as illustrated in Fig. 1.

The classical expansion from two-scale homogenization theory studied extensively (Panasenko, 2005; Boughammoura, 2013) seeks in our case solutions u^ϵ to (1) in the form:

$$u^\epsilon(\mathbf{x},t) = u^0(\mathbf{x},t) + \epsilon N^{rs}(\frac{\mathbf{x}}{\epsilon})\mathbf{e}_{rs}\big(u^0(\mathbf{x},t)\big) + r^\epsilon(\mathbf{x},t,\epsilon), \tag{2}$$

where r^ϵ is some error term and we use the standard notation $N^{rs}(\mathbf{y})$ to describe cell solutions to the so-called cell problems defined as the elliptic PDE system:

$$\begin{aligned} -\partial_{y_j}\big(C_{ijkl}(\mathbf{y})\mathbf{e}_{kl}(N^{rs}(\mathbf{y}))\big) &= \partial_{y_j}\big(C_{ijrs}(\mathbf{y})\big) \quad \text{in} \quad \mathbf{Y}, \\ C_{ijkl}(\mathbf{y})\mathbf{e}_{kl}\big(N^{rs}(\mathbf{y})\big)n_j &= \mathbf{0} \quad \text{on} \quad \partial\mathbf{Y}, \\ \textstyle\int_{\mathbf{Y}} N^{rs}(\mathbf{y})\,d\mathbf{y} &= \mathbf{0}. \end{aligned} \tag{3}$$

Such cell problems enables the definition of the so-called homogenized elastic coefficients C^{hom}_{ijkl}, that incorporates the intrinsic nonlinearity arising from the microstructure, described by the integral form:

$$C^{hom}_{ijrs} = \frac{1}{|\mathbf{Y}|}\int_{\mathbf{Y}}\big(C_{ijrs}(\mathbf{y}) + C_{ijkl}\mathbf{e}_{kl}\big(N^{rs}(\mathbf{y})\big)\big)\,d\mathbf{y}, \tag{4}$$

in which at the macroscopic scale, the solution u^0 satisfies the homogenized linear-elastic PDE system with the homogeneous coefficients:

$$\begin{aligned} \rho^0\partial_{tt}u^0(\mathbf{x},t) - \nabla\cdot\sigma^0(\mathbf{x},t) &= \mathbf{f}(\mathbf{x},t) \quad \text{in} \quad \Omega\times(0,T), \\ \sigma^0_{ij}(\mathbf{x},t) &= C^{hom}_{ijkl}\mathbf{e}_{kl}(u^0(\mathbf{x},t)) \quad \text{in} \quad \Omega\times(0,T), \end{aligned} \tag{5}$$

where mass density satisfies $\rho^0 = \frac{1}{|\mathbf{Y}|}\int_{\mathbf{Y}}\rho(\mathbf{y})d\mathbf{y}$, with the same original boundary conditions. For the deduction of the homogenized model, i.e., Eqs. (3) to (5), see for instance Bakhvalov and Panasenko (1989).

2.2. Mechanical assumptions

Following the standard biomechanical literature, both phases, solid (collagen and hydroxyapatite matrix) and fluid (saturated porous-like inclusions) are assumed to follow a linear elastic behavior. Taking axial symmetry along the long axis of bone, the composite material is modeled with transverse isotropy for each tensor component C^m_{ijkl}, C^f_{ijkl} associated with the bone matrix and the material inside the pores respectively. Thus, the elastic coefficients on the cell $\mathbf{Y}$ are described in the form:

$$C_{ijkl}(\mathbf{y}) := C^m_{ijkl}\mathbb{I}_{\{\mathbf{y}\in\mathbf{Y}_m\}} + C^f_{ijkl}\mathbb{I}_{\{\mathbf{y}\in\mathbf{Y}_f\}}. \tag{6}$$

Such component-wise elastic behavior is described explicitly using *Voigt* notation as the following square matrix with coefficients (Parnell et al., 2012):

$$C_{ij}(\mathbf{y}) = \begin{bmatrix} C_{11}(\mathbf{y}) & C_{12}(\mathbf{y}) & C_{13}(\mathbf{y}) & 0 & 0 & 0 \\ C_{12}(\mathbf{y}) & C_{11}(\mathbf{y}) & C_{13}(\mathbf{y}) & 0 & 0 & 0 \\ C_{13}(\mathbf{y}) & C_{13}(\mathbf{y}) & C_{33}(\mathbf{y}) & 0 & 0 & 0 \\ 0 & 0 & 0 & C_{44}(\mathbf{y}) & 0 & 0 \\ 0 & 0 & 0 & 0 & C_{44}(\mathbf{y}) & 0 \\ 0 & 0 & 0 & 0 & 0 & C_{66}(\mathbf{y}) \end{bmatrix},$$

associated to a transverse isotropic material with the axis 3 corresponding to the bone axis, implying that: $C_{55}(\mathbf{y}) = C_{44}(\mathbf{y})$ and $C_{11}(\mathbf{y}) = C_{22}(\mathbf{y})$. Moreover, we also assumed $C_{12}(\mathbf{y}) = C_{11}(\mathbf{y}) - 2C_{66}(\mathbf{y})$ as in Bernard et al. (2016). Thus, the bone matrix part can be described using five independent coefficients, C^m_{11}, C^m_{33}, C^m_{44}, C^m_{66} and C^m_{13}.

The material inside the pores is supposed isotropic, implying $C^f_{11} = C^f_{22} = C^f_{33}$ and $C^f_{44} = C^f_{55} = C^f_{66}$. Non diagonal terms are given by $C^f_{12} = C^f_{13} = C^f_{23} = C^f_{11} - 2C^f_{44}$. Thus, the material inside the pore can be described using two independent coefficients, C^f_{11} and C^f_{44}. In this setting, the homogenized coefficients are defined as functions of the porosity level, i.e. setting the cylindrical inclusion in a unitary cube (3D cell) with radius $r(p)$, being $p \in (0,1)$ the range of admissible porosity levels, in the form $p := \frac{|\mathbf{Y}_f|}{|\mathbf{Y}|}$ The circular fluid inclusion $\mathbf{Y}_f$ is illustrated in Fig. 1. The homogenized mass density is defined as $\rho^{hom} = \rho^m(1-p) + \rho^f p$ (Parnell and Grimal, 2009). Note that other geometry of cell problems, such as hexagonal, have been considered for composite (Penta and Gerisch, 2015), poroelastic (Dehghani et al., 2018) or cortical bone (Parnell and Grimal, 2009) materials.

2.3. Viscoelastic model

The damping effects observed on experimental signals reveal the presence of viscous-like behavior that should be addressed to correctly predict the mechanical behavior of cortical bone. In this section we propose a generalization of the linear elastic mechanical model of bone to a *Kelvin–Voigt* viscoelastic behavior within the two-scale framework, which to our knowledge corresponds to the first formal deduction of such factors using this approach. Cortical bone relaxation times are of the order of the second, very large compared to the typical period considered in this study, i.e., 10 μs at 0.1 MHz (Iyo et al., 2004; Yamashita et al., 2001; Wu et al., 2012). Thus, more sophisticated viscoelastic models such as *Maxwell* model, are not required in the present case (Yi et al., 1998; Abdessamad et al., 2009; Nguyen et al., 2018; Cruz González et al., 2020).

As in Section 2.1, we consider a *Kelvin–Voigt* model for the cortical bone behavior, characterized by elastic $C^\epsilon_{ijkl}(\mathbf{x})$ and viscoelastic $D^\epsilon_{ijkl}(\mathbf{x})$ tensors that define a solution $u^\epsilon(\mathbf{x},t)$ as

$$\begin{aligned} \rho^\epsilon(\mathbf{x})\partial_{tt}u^\epsilon(\mathbf{x},t) - \nabla\cdot\hat{\sigma}^\epsilon(\mathbf{x},t) &= \mathbf{f}(\mathbf{x},t) && \text{in} \quad \Omega\times(0,T),\\ \hat{\sigma}^\epsilon_{ij}(\mathbf{x},t) = C^\epsilon_{ijkl}(\mathbf{x})\mathbf{e}_{kl}(u^\epsilon(\mathbf{x},t)) + D^\epsilon_{ijkl}(\mathbf{x})\mathbf{e}_{kl}(\partial_t u^\epsilon(\mathbf{x},t)) &&\text{in} \quad \Omega\times(0,T), \end{aligned} \tag{7}$$

Now if we put a fixed positive angular pulsation ω and $u^\epsilon(\mathbf{x},t) = \hat{u}^\epsilon(\mathbf{x})e^{i\omega t}$ and $\mathbf{f}(\mathbf{x},t) = \hat{\mathbf{f}}(\mathbf{x})e^{i\omega t}$, we arrive to the following problem for $\hat{u}^\epsilon(\mathbf{x})$:

$$\begin{aligned} -\omega^2\rho^\epsilon(\mathbf{x})\hat{u}^\epsilon(\mathbf{x}) - \nabla\cdot\hat{\sigma}^\epsilon(\mathbf{x}) &= \hat{\mathbf{f}}(\mathbf{x}) && \text{in} \quad \Omega,\\ \hat{\sigma}^\epsilon_{ij}(\mathbf{x}) = \left(C^\epsilon_{ijkl}(\mathbf{x}) + \mathbf{i}\omega D^\epsilon_{ijkl}(\mathbf{x})\right)\mathbf{e}_{kl}(\hat{u}^\epsilon(\mathbf{x})) &&\text{in} \quad \Omega. \end{aligned} \tag{8}$$

where again $\rho^\epsilon(\mathbf{x}) = \rho(\mathbf{x}/\epsilon)$, $C^\epsilon_{ijkl}(\mathbf{x}) = C_{ijkl}(\mathbf{x}/\epsilon)$ and $D^\epsilon_{ijkl}(\mathbf{x}) = D_{ijkl}(\mathbf{x}/\epsilon)$ are the periodic density, elastic and viscoelastic parameters and with the same boundary conditions as for the original model (1).

By expressing the solution $\hat{u}^\epsilon$ as an asymptotic expansion in ϵ, it is straightforward to deduce the cell problems, that generalize the elastic case, described by solutions $\hat{N}^{rs}(\mathbf{y})$ to the elliptic system:

$$\begin{aligned} -\partial_{y_j}\left[\left(C_{ijkl}(\mathbf{y}) + \mathbf{i}\omega D_{ijkl}(\mathbf{y})\right)\mathbf{e}_{kl}(\hat{N}^{rs}(\mathbf{y}))\right],&\\ \quad = \partial_{y_j}\left[C_{ijrs}(\mathbf{y}) + \mathbf{i}\omega D_{ijrs}(\mathbf{y})\right] && \text{in} \quad \mathbf{Y},\\ \left(C_{ijkl}(\mathbf{y}) + \mathbf{i}\omega D_{ijkl}(\mathbf{y})\right)\mathbf{e}_{kl}(N^{rs}(\mathbf{y}))n_j = \mathbf{0} && \text{on} \quad \partial\mathbf{Y},\\ \int_{\mathbf{Y}}\hat{N}^{rs}(\mathbf{y})\,d\mathbf{y} = \mathbf{0}. \end{aligned} \tag{9}$$

Now we decouple the solution of this system by splitting the cell solution into the form:

$$\hat{N}^{rs}(\mathbf{y}) = \hat{N}^{rs}_R(\mathbf{y}) + \mathbf{i}\hat{N}^{rs}_I(\mathbf{y}), \tag{10}$$

being each vector valued function $\hat{N}^{rs}_R, \hat{N}^{rs}$ solution of a real valued coupled cell problem.

Using this decomposition, from the expression of $C^{hom}_{ijrs} + \mathbf{i}\omega D^{hom}_{ijrs}$ similar to (4), it is easy to see by taking real and imaginary parts that the homogenized elastic and viscous coefficients are given by the following integral expressions:

$$\begin{aligned} C^{hom}_{ijrs} &= \frac{1}{|\mathbf{Y}|}\int_{\mathbf{Y}} C_{ijrs}(\mathbf{y}) + \left(C_{ijkl}(\mathbf{y})\mathbf{e}_{kl}(\hat{N}^{rs}_R(\mathbf{y})) - \omega D_{ijkl}(\mathbf{y})\mathbf{e}_{kl}(\hat{N}^{rs}_I(\mathbf{y}))\right)d\mathbf{y},\\ D^{hom}_{ijrs} &= \frac{1}{|\mathbf{Y}|}\int_{\mathbf{Y}} D_{ijrs}(\mathbf{y})\\ &\quad + \left(\omega^{-1}C_{ijkl}(\mathbf{y})\mathbf{e}_{kl}(\hat{N}^{rs}_I(\mathbf{y})) + D_{ijkl}(\mathbf{y})\mathbf{e}_{kl}(\hat{N}^{rs}_R(\mathbf{y}))\right)d\mathbf{y}, \end{aligned} \tag{11}$$

where the macroscopic homogenized viscoelastic behavior is described by the solution $\hat{u}^0$ of the problem:

$$\begin{aligned} -\omega^2\rho^0\hat{u}^0(\mathbf{x}) - \nabla\cdot\hat{\sigma}^0(\mathbf{x}) &= \mathbf{f}(\mathbf{x}) && \text{in } \Omega,\\ \hat{\sigma}^0_{ij}(\mathbf{x}) = \left(C^{hom}_{ijkl} + \mathbf{i}\omega D^{hom}_{ijkl}\right)\mathbf{e}_{kl}\left(\hat{u}^0(\mathbf{x})\right) &&\text{in } \Omega, \end{aligned} \tag{12}$$

where again $\rho^0 = \frac{1}{|\mathbf{Y}|}\int_{\mathbf{Y}}\rho(\mathbf{y})d\mathbf{y}$ and with the same boundary conditions as in the original viscoelastic model (7).

2.4. Introduction of the Q and τ factors

The definition of quality factors Q_{ijkl} proposed in (Bernard et al., 2016) can be deduced directly in the homogenized framework from the system (12) in the form:

$$(Q^{hom}_{ijkl})^{-1}(\omega) := \omega\frac{D^{hom}_{ijkl}}{C^{hom}_{ijkl}} = \omega\tau^{hom}_{ijkl}, \tag{13}$$

for each angular pulsation ω of interest. With Q being dimensionless, the ratio between D and C coefficients is homogeneous up to a temporal factor, denoted τ in the following.

Regarding the phase composition of the microstructure $\mathbf{Y}$, we model the viscous coefficients analogous to Eq. (6) in the form:

$$D_{ijkl}(\mathbf{y}) = D^m_{ijkl}\mathbb{I}_{\{\mathbf{y}\in\mathbf{Y}_m\}} + D^f_{ijkl}\mathbb{I}_{\{\mathbf{y}\in\mathbf{Y}_f\}}, \tag{14}$$

and we define such viscous coefficients $(D_{ijkl})_{ijkl}$ as linearly attenuated of its elastic counterparts with parameters $(Q^m_{ijkl})^{-1}(\omega) > 0$ and $(Q^f_{ijkl})^{-1}(\omega) > 0$ for the matrix and fluid phases respectively. More explicitly, we assume that:

$$\begin{aligned} \omega D^m_{ijkl}(\mathbf{y}) &= (Q^m_{ijkl})^{-1}(\omega)C^m_{ijkl}(\mathbf{y}),\\ \omega D^f_{ijkl}(\mathbf{y}) &= (Q^f_{ijkl})^{-1}(\omega)C^f_{ijkl}(\mathbf{y}). \end{aligned} \tag{15}$$

Let us note that by assuming such type of relation for the viscoelastic description, we limit the amount of degrees of freedom on the model, to facilitate the study of the dependence and effects of each controlled parameter.

2.5. Simplified model

The definitions of the two tensors $D^m_{ijkl}(\mathbf{y})$ and $D^f_{ijkl}(\mathbf{y})$, associated with the matrix and fluid phases respectively, are furthermore simplified using proportionality factors τ^m and τ^f as:

$$\begin{aligned} \omega D^m_{ijkl}(\mathbf{y}) &= \omega\tau^m C^m_{ijkl}\mathbb{I}_{\{\mathbf{y}\in\mathbf{Y}_f\}},\\ \omega D^f_{ijkl}(\mathbf{y}) &= \omega\tau^f C^f_{ijkl}\mathbb{I}_{\{\mathbf{y}\in\mathbf{Y}_f\}}. \end{aligned} \tag{16}$$

Combining (15) and (16) , it is possible to express the bone matrix and fluid quality factors as $(Q^m)^{-1}(\omega)$ and $(Q^f)^{-1}(\omega)$ as $\omega\tau^m$ and $\omega\tau^f$, respectively (Abdessamad et al., 2009). The τ factor and can be interpreted as a typical time constant. Thus, if the frequency f is expressed in MHz, then τ is in μs. Note that the condition $Q^{-1} = \omega\tau \ll 1$ corresponds to a weak attenuation case for which the time constant τ is small compared to the period $T = 2\pi/\omega$.

Ultrasonic attenuation is usually modeled using a power law (Szabo, 1995; Holm, 2019), and a complex wavenumber $k + i\alpha$. In case of weak attenuation, i.e., $\alpha \ll k$, the quality factor Q^{-1} is about $2\alpha/k$.

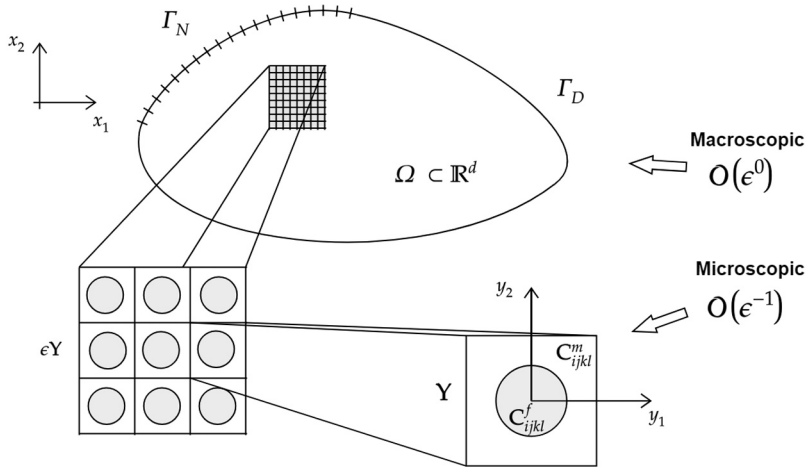

Fig. 1. Cortical bone is represented as a composite material, using a two-scale assumption for the microstructure and matrix/hard C^m_{ijkl} and fluid/soft C^f_{ijkl} elastic coefficients, periodically distributed along the long bone axis x_3. The 3D-periodic cell is a fluid filled cylinder included in a unitary cube.

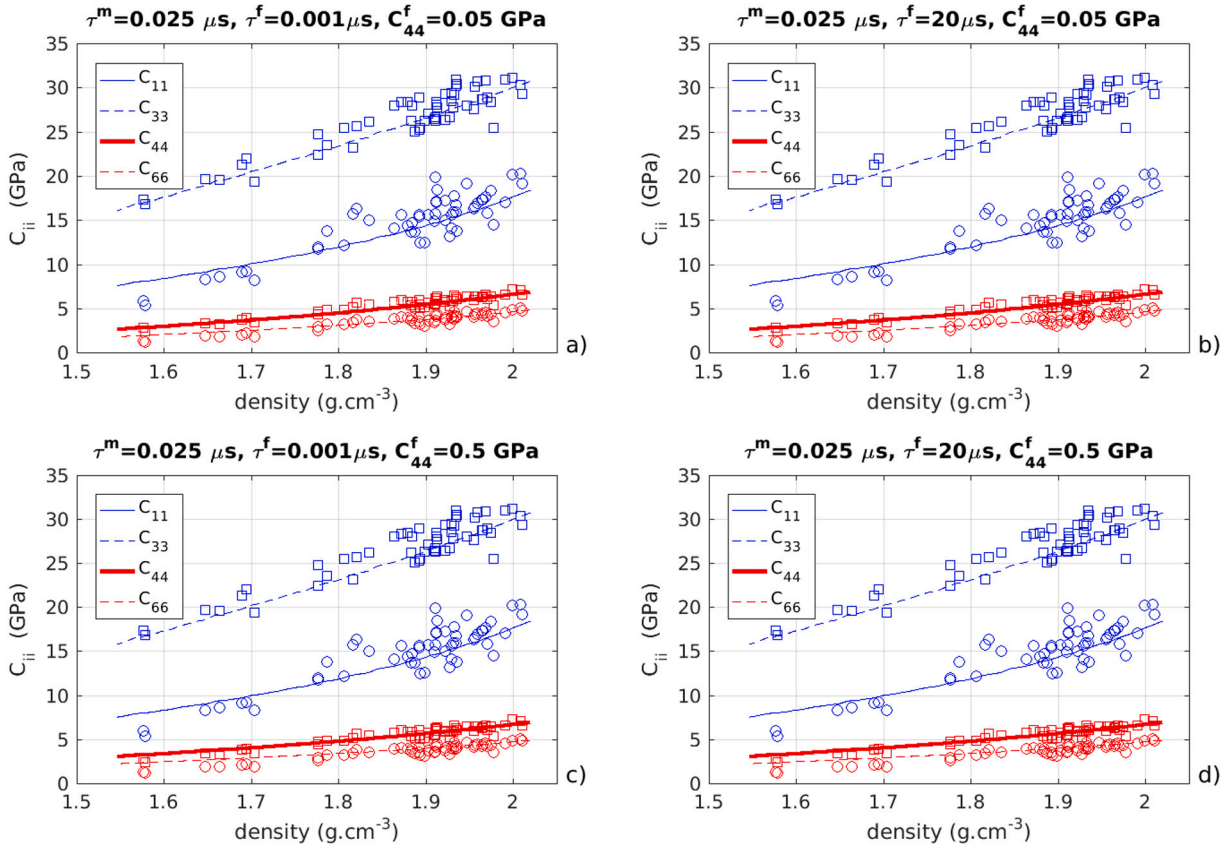

Fig. 2. Real part of the stiffness coefficients C_{ii} factors obtained experimentally in Bernard et al. (2016) (dots), compared against our numerical predictions (FEM, lines), computing the factors C_{ii}. In prediction interval is given at high density values, i.e., lower porosity levels where the bigger data samples are available. The four cases are: Soft tissue with weak attenuation (a), soft tissue with strong attenuation (b), solid with weak attenuation (c) and solid with strong attenuation (d).

With $Q^{-1} = \omega\tau$, the attenuation is then proportional to the square of frequency as:

$$\alpha(\omega) \approx \frac{1}{2}\frac{\tau}{c_0}\omega^2, \tag{17}$$

with c_0 the low frequency limit bulk velocity. Note that Eq. (17) is similar to Eq. (30a) derived by O'Donnell et al. (1981) from Kramers–Kronig relationship between ultrasonic attenuation and phase velocity.

2.6. Domain of validity

Following homogenization theory in elasticity with contrasting coefficients (see for instance Panasenko, 2005 and Sandrakov, 1999), if κ

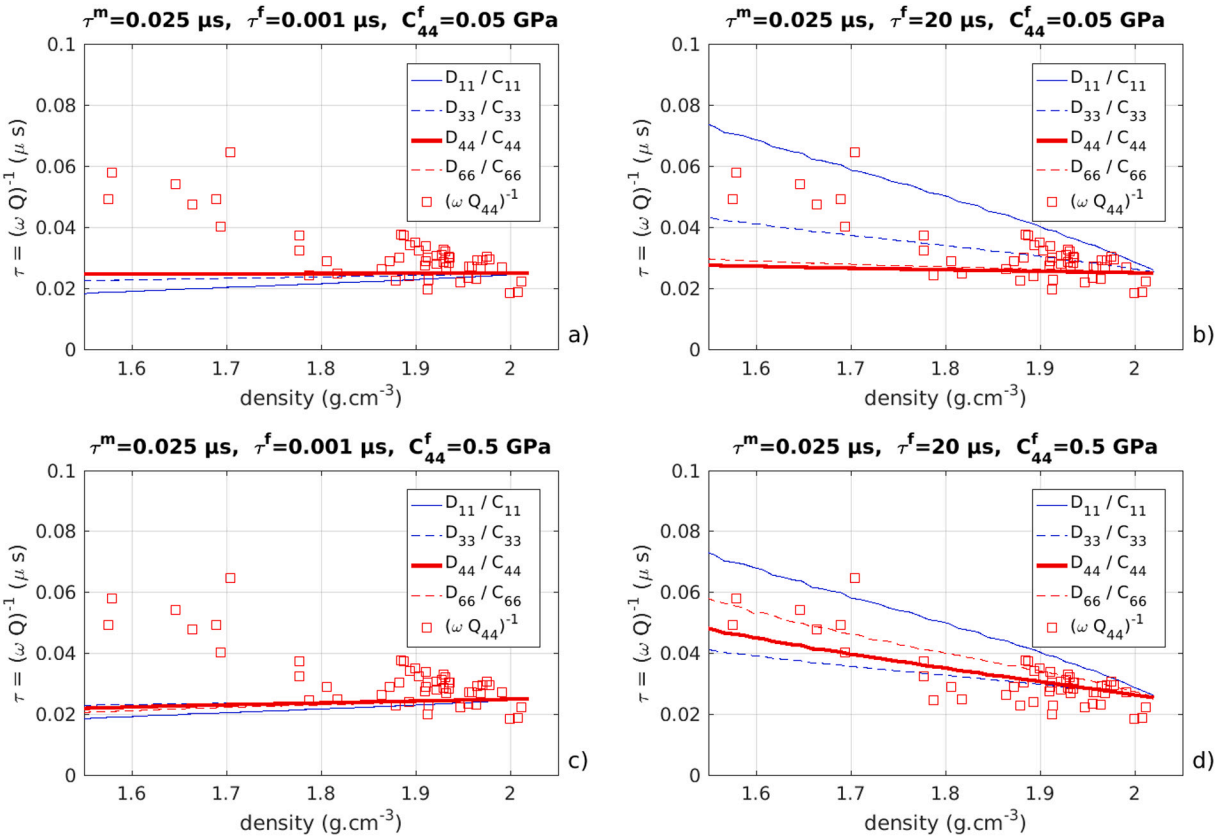

Fig. 3. Homogenized factor $\tau^{hom} = (\omega Q)^{-1}$ factors obtained with numerical predictions (FEM, lines), computing the factors D_{ii} C_{ii}, compared obtained experimentally in (Bernard et al., 2016) (dots) for direction 44. In prediction interval is given at high density values, i.e., lower porosity levels where the bigger data samples are available. The four cases are: Soft tissue with weak attenuation (a), soft tissue with strong attenuation (b), solid with weak attenuation (c) and solid with strong attenuation (d).

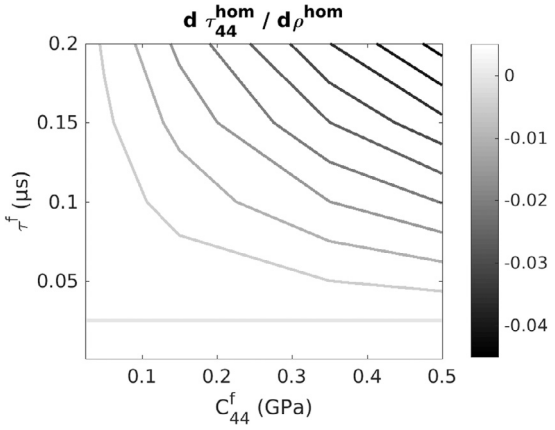

Fig. 4. Homogenized slope $d\tau^{hom}/d\rho^{hom}$ calculated for different combinations of τ^f and C^f_{44} values.

is the elastic contrast that could be estimated by:

$$\kappa = max_i \frac{C^m_{ii}}{C^f_{ii}}, \tag{18}$$

if ε is the homogenization parameter, then if $\kappa\,\varepsilon^2$ is small, the homogenization regime approximation is valid. In our case, these values correspond to $\kappa \approx 30$ GPa/2 GPa $= 15$ and $\varepsilon \approx 50$ µm/1 mm $= 0.05$ giving $\kappa\,\varepsilon^2 \approx 0.04$. Otherwise, in case of large pore or higher elastic contrast, a more involved homogenization process called multi-component homogenization should be used (Panasenko, 2005).

3. Numerical simulations

The implementation of the variational formulation in (3) is done using the state-of-art library `FEniCS` for the cubic microstructure **Y** including a cylindrical pore on 3-dimensional settings as described on Fig. 1 (Logg and Wells, 2010; Logg, 2012). The discretization procedure associated to the variational formulation is obtained by Finite Element Method and solved using `GMRES` (Generalized Minimal Residual Method) with preconditioner `iLU` (incomplete lower–upper factorization) to tackle the numerical instabilities obtained from the inversion of the linear system. The viscoelastic extension is done by defining a unit cubic microstructure **Y** where the integral formulations (11) are computed by FEM. The *Kelvin–Voigt* model described in 2.3 is then simulated and the derived stiffness coefficients and temporal factors are then compared to available experimental data (Bernard et al., 2016).

The numerical values of the bone matrix elasticity used in this study are equal to (in GPa): $C^m_{11} = 18.7$, $C^m_{33} = 31.0$, $C^m_{44} = 7.0$, $C^m_{66} = 4.9$, $C^m_{13} = 10.1$ (Bernard et al., 2016). The reference fluid values are equal to (in GPa): $C^f_{11} = 2.05$ and $C^f_{44} = 0.025$. The mass densities ρ^m and ρ^f are equal to 1.91 an 1.0 g cm^{-3}, for the bone matrix and fluid parts respectively (Granke et al., 2011). The value of τ^m is fixed equal to 0.025 µs, while the reference value of τ^f is fixed to 0.001 µs. With typical frequencies ranging from 100 to 300 kHz, the factor ω ranges from about 0.5 to 2 rad µs^{-1}. In the following, ω is fixed to 1 rad µs^{-1}. Note that different values of ω have been tested providing the same values for the coefficients τ^{hom}. In order to explore different

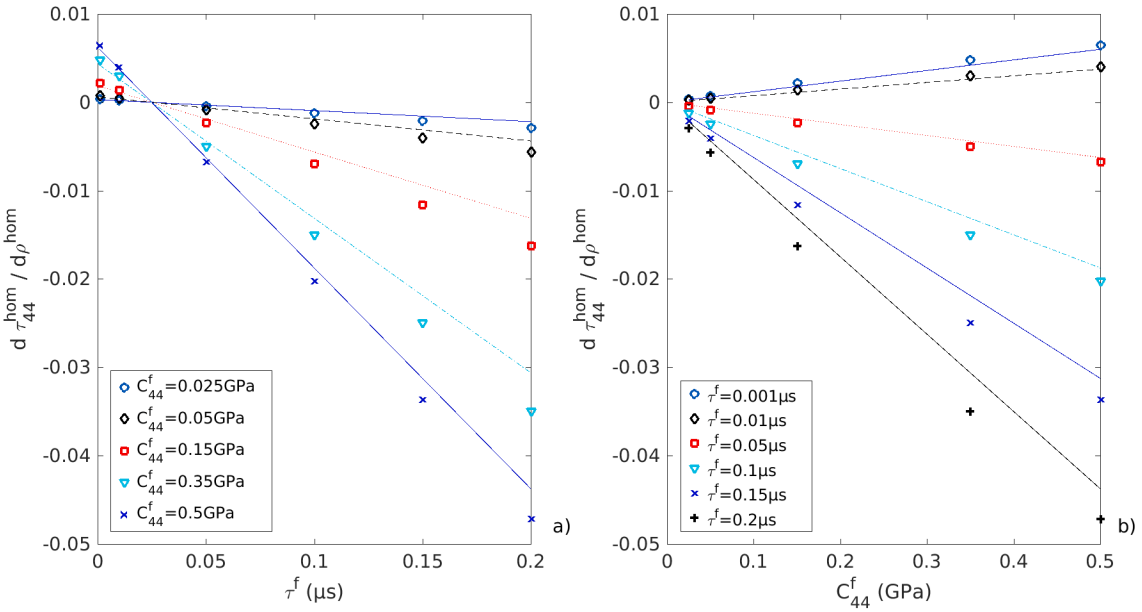

Fig. 5. Homogenized slope $d\tau^{hom}/d\rho$ vs τ^f (a) and C_{44}^f (b) compared with the approximated values given by Eq. (19).

configurations, the two coefficients τ^f and C_{44}^f will range reference values, i.e., a weakly attenuating ($\omega\tau^f \ll 1$) soft tissue ($C_{44}^f \ll C_{11}^f$) to a strongly attenuating ($\tau^f = 0.2$ μs) solid ($C_{44}^f = 0.5$ GPa).

In a first approach, four limit cases are considered for the material inside the pores: soft tissue with weak attenuation (a), soft tissue with strong attenuation (b), solid with weak attenuation (c) and solid with strong attenuation (d). The real part of the homogenized stiffness coefficients are shown in Fig. 2 in function of the homogenized density. One can observe that the results are slightly affected by the changing of parameters of the four different cases and that the homogenized stiffness coefficients are in agreement with the experimental data, in agreement with previous results shown in (Bernard et al., 2016).

Then, the homogenized τ^{hom} factors are shown in Fig. 3, also in function of the homogenized density. In this case, the changing of parameters is associated with a modification of the changing in the slope of the curves. In all case, at low porosity or large density, the homogenized τ^{hom} factor tends to the value of the matrix alone, i.e., $\tau^m = 0.025$ μs. In cases (a) and (c) of weak attenuation, variations of τ^{hom} are small. On the contrary, in cases (b) and (d) of large attenuation, variations of τ^{hom} are larger. However, in case (b) of soft tissue with strong attenuation, τ^{hom} variations are weaker for shear coefficients (44 and 66) than for longitudinal coefficients (11 and 33). Finally, in case (d) of solid with strong attenuation, τ^{hom} variations with density are strong for both shear and longitudinal contributions. The best agreement with experimental data (τ_{44}) is obtained for this last case.

In a second approach, models associated with different combinations of values of τ_f and C_{44}^f within the previously mentioned ranges are computed. The values of the slopes $d\tau_{44}^{hom}/d\rho^{hom}$ are reported in Figs. 4 and in Fig. 5. In the last figure, values are and compared with the following heuristic linear approximation:

$$\tau_{44}^{hom} \approx \tau^m + \frac{1}{2}\rho^{hom}(\tau^m - \tau^f)C_{44}^f. \tag{19}$$

4. Discussion

This paper describes the inclusion of the attenuation into a homogenized model, introducing a typical time τ linked to the frequency and the quality factor as $Q^{-1} = \omega\tau$, using a *Kelvin–Voigt* type behavior with damping effects characterized via anisotropic attenuation of the elastic coefficients. To our knowledge is the first time that this point of view is applied to cortical bone. Similar previous works focused on the real part of the stiffness coefficient C_{ij} (Parnell and Grimal, 2009; Parnell et al., 2012). Attenuation have been studied at lower frequencies, less than 1 kHz for vibro acoustic application, scanning the complete bone (Aygün, 2019). Attenuation has also been recently studied for higher frequency range, 1 to 8 MHz, using FDTD simulations (Yousefian et al., 2021), showing the measured attenuation depends not only on porosity but also on the size and distribution of the pores. On the contrary, within the homogenization frame, results are not influenced by the pore distribution. It can be noted that the present work is devoted to the medium frequency range, from about 10 kHz to 1 MHz, when typical wavelength about a few millimeters are larger than the mesoscale typical size, about 100 micrometers.

One of the main interest of this approach is to describe the global or homogenized behavior as a mix of each part, in the cortical bone case, bone matrix and fluid. In particular, the model predicts that in case of weakly attenuated fluid ($\tau^f = 0.001$ μs), the homogenized τ^{hom} will decrease with porosity. It can be understood as porosity increases, more fluid is added to the mix, and the fluid has a lower attenuation than the cortical bone matrix ($\tau^m = 0.025$ μs). However, this behavior is not in agreement with the observed experimental results, for which the τ^{hom} increases with porosity or decreased with mass density (Bernard et al., 2016). In order to obtain a good agreement between the model and the experiments, two main modifications were made: first increase the attenuation and then increase the shear coefficient. Indeed, in the first case, only the attenuation of the longitudinal coefficients 11 and 33, increased with porosity. In conclusion, according to homogenization, pores should be filled with a highly attenuated solid in order to observe a good agreement. One the one hand, to this date only a few experimental values are available. Values should be comforted with other studies. One the other hand, this point may be explained by microfluidic experiments taking into account the size and form of the pores (Galindo-Rosales et al., 2011). It can be supposed that the fluid behavior is different in small pores than in bulk conditions, without boundary interactions.

Values observed in this study can be compared with typical values obtained for cortical bone in previous studies, using power law (Szabo, 1995; Holm, 2019). The case of order 2 relation, derived from Kramer–Kronig relations has been used for bone marrow (Kawasaki et al., 2015). If the coefficient α writes as $\alpha_0 f^2$, the typical time τ^f is then $\alpha_0 c_0^f/(2\pi^2)$. With α_0 equal to 0.04 dB cm^{-1} MHz^{-2} and c_0^f equal to

1.4 mm.μs^{-1}, τ^f is about 3.10^{-5} μs. The case of order 1 relation corresponds to the slope of a Taylor expansion around the frequency of interest and is usually used for cortical bone (Sasso et al., 2008; Minonzio et al., 2021). If the coefficient α writes as βf, the factor $\omega\tau^m$ is about $\beta c_0^m/\pi$. Note that a recent simulations study suggested that an order 2 relation is also adapted for cortical bone at frequencies higher than 1 MHz (Yousefian et al., 2021). In the experimental data used in this study (Bernard et al., 2016), the measured frequencies ranged from 100 to 300 kHz, implying that the angular pulsation ω ranged from 0.6 to 1.9 rad μs^{-1}. The limit τ value for high density or low density is about 0.025 μs or 4 dB cm^{-1} MHz^{-1}, with ω equal 1 and v_{44}^m equal 1.8 mm μs^{-1}. Likewise, the largest experimental τ value, corresponding to the largest porosity values, is about 0.06 μs or 10 dB cm^{-1} MHz^{-1}. These values are within the range of attenuation values measured *ex vivo* (Sasso et al., 2008) in cortical bone, even if the number of experimental studies are currently small.

The idea behind this simplified model is to take into account viscoelasticity in robust clinical inverse problem. For example, homogenized elasticity has been used to develop a two parameters, cortical thickness and porosity, approach associated with guided wave measurements (Minonzio et al., 2019). In that case, stiffness coefficients of both phases are considered known. Further work will concern the addition of one unique attenuation parameter τ^m to the inverse problem. For example, τ could be studied in comparison with relaxation times (Kawada et al., 2006; Holm, 2019). Another approach would be to include attenuation into multi scale, not only two, asymptotic homogenization (Ramírez-Torres et al., 2018), as global attenuation could result from different phenomena, associated with different scales. Multi-component homogenization could also be studied in case of large pores when the regime $\kappa\epsilon^2 \ll 1$ is not verified (Panasenko, 2005). Finally, the role of mineralization should be taken into account in addition to cortical porosity.

5. Conclusion

We conclude from this numerical study about characterization of the viscoelastic behavior in cortical bone via two-scale homogenization, that microscopic structures with transverse isotropic assumption parametrized with porosity lead to realistic predictions of both real and imaginary part of stiffness coefficients when compared with experimental data. This model should indeed be improved by taking into account for example the variation of mineralization of the bone matrix, the shape of the porous canals and the fluid behavior at small scale. This works opens perspective towards novel ultrasonic clinical parameters associated with cortical bone attenuation and its ability to absorb shock, such as quality Q and temporal τ factors.

CRediT authorship contribution statement

Reidmen Aróstica: Formal analysis, Programming, Original draft, Review & editing. **Ana Aguilera:** Programming; Code testing, Validation, Review & editing. **Axel Osses:** Formal analysis, Supervision, Project administration, Funding acquisition, Review & editing. **Jean-Gabriel Minonzio:** Dimensional analysis, Supervision, Project administration, Funding acquisition, Original draft, Review & editing.

Declaration of competing interest

The authors declare that they have no known competing financial interests or personal relationships that could have appeared to influence the work reported in this paper.

Acknowledgments

Jean-Gabriel Minonzio (JGM) and Axel Osses (AO) are supported by ANID-Fondecyt Regular Grant 1201311 and ECOS 200061. AO was partially funded by ANID-Fondecyt Regular Grant 1191903, Basal Program CMM-AFB 170001, FONDAP/15110009, Millennium Science Iniciative Programs NCN17_1 and NCN19_161, Math-Amsud Project ACIPDE MATH190008. Authors would like to thanks Grigory Panasenko for his advices and Quentin Grimal for sharing of the experimental values.

References

Abdessamad, Z., Kostin, I., Panasenko, G., Smyshlyaev, V.P., 2009. Memory effect in homogenization of a viscoelastic Kelvin-Voigt model with time-dependent coefficients. Math. Models Methods Appl. Sci. 19 (09), 1603–1630. http://dx.doi.org/10.1142/s0218202509003905.

Ahmed, L., Shigdel, R., Joakimsen, R., Eldevik, O., Eriksen, E., Ghasem-Zadeh, A., Bala, Y., Zebaze, R., Seeman, E., Bjørnerem, A., 2015. Measurement of cortical porosity of the proximal femur improves identification of women with nonvertebral fragility fractures. Osteoporos. Int. 26, http://dx.doi.org/10.1007/s00198-015-3118-x.

Akhter, M., Recker, R., 2021. High resolution imaging in bone tissue research-review. Bone 143, 115620. http://dx.doi.org/10.1016/j.bone.2020.115620.

Aygün, H., 2019. A viscoelastic system for determining acoustical and mechanical parameters of the bone. Appl. Acoust. 150, 70–75. http://dx.doi.org/10.1016/j.apacoust.2019.01.034.

Bakhvalov, N., Panasenko, G., 1989. Homogenisation: Averaging Processes in Periodic Media: Mathematical Problems in the Mechanics of Composite Materials, Chapter 4. Averaging Basic Equations of Mathematical Physics. Springer Netherlands, Dordrecht.

Bernard, S., Schneider, J., Varga, P., Laugier, P., Raum, K., Grimal, Q., 2016. Elasticity–density and viscoelasticity–density relationships at the tibia mid-diaphysis assessed from resonant ultrasound spectroscopy measurements. Biomech. Model. Mechanobiol. 15 (1), 97–109. http://dx.doi.org/10.1007/s10237-015-0689-6.

Bjørnerem, A., 2016. The clinical contribution of cortical porosity to fragility fractures. BoneKEy Rep. 5, 846. http://dx.doi.org/10.1038/bonekey.2016.77.

Boughammoura, A., 2013. Homogenization of a highly heterogeneous elastic-viscoelastic composite materials. Mediterr. J. Math. 10 (4), 1793–1812. http://dx.doi.org/10.1007/s00009-013-0262-4.

Cai, X., Brenner, R., Peralta, L., Olivier, C., Gouttenoire, P.-J., Chappard, C., Peyrin, F., Cassereau, D., Laugier, P., Grimal, Q., 2019. Homogenization of cortical bone reveals that the organization and shape of pores marginally affect elasticity. J. R. Soc. Interface 16, http://dx.doi.org/10.1098/rsif.2018.0911.

Cruz González, O.L., Ramírez-Torres, A., Penta, R., Bravo-Castillero, J., Guinovart-Díaz, R., Merodio, J., Sabina, F., Lebon, F., 2020. A hierarchical asymptotic homogenization approach for viscoelastic composites. Mech. Adv. Mater. Struct. 1–12. http://dx.doi.org/10.1080/15376494.2020.1722872.

Dehghani, H., Penta, R., Merodio, J., 2018. The role of porosity and solid matrix compressibility on the mechanical behavior of poroelastic tissues. Mater. Res. Express 6, http://dx.doi.org/10.1088/2053-1591/aaf5b9.

Fan, Z., Rho, J.-Y., 2003. Effects of viscoelasticity and time-dependent plasticity on nanoindentation measurements of human cortical bone. J. Biomed. Mater. Res. A 67A (1), 208–214. http://dx.doi.org/10.1002/jbm.a.10027.

Gagliardi, D., Sansalone, V., Desceliers, C., Naili, S., 2018. Estimation of the effective bone-elasticity tensor based on μ CT imaging by a stochastic model. A multi-method validation. Eur. J. Mech. A Solids 69, 147–167. http://dx.doi.org/10.1016/j.euromechsol.2017.10.004.

Galindo-Rosales, F., Campo-Deaño, L., Pinho, F., van Bokhorst, E., Hamersma, P., Oliveira, M., Alves, M., 2011. Microfluidic systems for the analysis of viscoelastic fluid flow phenomena in porous media. Microfluid. Nanofluid. 12, 485–498. http://dx.doi.org/10.1007/s10404-011-0890-6.

Granke, M., Gourrier, A., Rupin, F., Raum, K., Peyrin, F., Burghammer, M., Saïed, A., Laugier, P., 2013. Microfibril orientation dominates the microelastic properties of human bone tissue at the lamellar length scale. PLOS ONE 8 (3), 1–11. http://dx.doi.org/10.1371/journal.pone.0058043.

Granke, M., Grimal, Q., Saïed, A., Nauleau, P., Peyrin, F., Laugier, P., 2011. Change in porosity is the major determinant of the variation of cortical bone elasticity at the millimeter scale in aged women. Bone 49, 1020–1026. http://dx.doi.org/10.1016/j.bone.2011.08.002.

Groetsch, A., Gourrier, A., Schwiedrzik, J., Sztucki, M., Beck, R.J., Shephard, J.D., Michler, J., Zysset, P.K., Wolfram, U., 2019. Compressive behaviour of uniaxially aligned individual mineralised collagen fibres at the micro- and nanoscale. Acta Biomater. 89, 313–329. http://dx.doi.org/10.1016/j.actbio.2019.02.053.

Hildebrand, K.N., Sidhu, K., Gabel, L., Besler, B.A., Burt, L.A., Boyd, S.K., 2021. The assessment of skeletal muscle and cortical bone by second-generation HR-pQCT at the tibial midshaft. J. Clinical Densitom. 24 (3), 465–473. http://dx.doi.org/10.1016/j.jocd.2020.11.001.

Holm, S., 2019. Waves with Power-Law Attenuation. Springer International Publishing, Switzerland, http://dx.doi.org/10.1007/978-3-030-14927-7.

Hong, A.L., Ispiryan, M., Padalkar, M.V., Jones, B.C., Batzdorf, A.S., Shetye, S.S., Pleshko, N., Rajapakse, C.S., 2019. MRI-derived bone porosity index correlates to bone composition and mechanical stiffness. Bone Rep. 11, 100213. http://dx.doi.org/10.1016/j.bonr.2019.100213.

Iori, G., Schneider, J., Reisinger, A., Heyer, F., Peralta, L., Wyers, C., Glüer, C.C., van den Bergh, J., Pahr, D., Raum, K., 2020. Cortical thinning and accumulation of large cortical pores in the tibia reflect local structural deterioration of the femoral neck. Bone 137, 115446. http://dx.doi.org/10.1016/j.mtla.2020.100730.

Ishimoto, T., Suetoshi, R., Cretin, D., Hagihara, K., Hashimoto, J., Kobayashi, A., Nakano, T., 2019. Quantitative ultrasound (QUS) axial transmission method reflects anisotropy in micro-arrangement of apatite crystallites in human long bones: A study with 3-MHz-frequency ultrasound. Bone 127, http://dx.doi.org/10.1016/j.bone.2019.05.034.

Iyo, T., Maki, Y., Sasaki, N., Nakata, M., 2004. Anisotropic viscoelastic properties of cortical bone. J. Biomech. 37 (9), 1433–1437. http://dx.doi.org/10.1016/j.jbiomech.2003.12.023.

Karjalainen, J., Riekkinen, O., Töyräs, J., Kröger, H., Jurvelin, J., 2008. Ultrasonic assessment of cortical bone thickness in vitro and in vivo. IEEE Trans. Ultrason. Ferroelectr. Freq. Control 55, 2191–2197. http://dx.doi.org/10.1109/TUFFC.918.

Kawada, Y., Nagahama, H., Hara, H., 2006. Irreversible thermodynamic and viscoelastic model for power-law relaxation and attenuation of rocks. Tectonophysics 427 (1), 255–263. http://dx.doi.org/10.1016/j.tecto.2006.03.049.

Kawasaki, S., Ueda, R., Hasegawa, A., Fujita, A., Mihata, T., Matsukawa, M., Neo, M., 2015. Ultrasonic wave properties of human bone marrow in the femur and tibia. J. Acoust. Soc. Am. 138 (1), EL83–EL87. http://dx.doi.org/10.1121/1.4922764.

Logg, A., 2012. Automated Solution of Differential Equations By the Finite Element Method : The FEniCS Book. Springer, Berlin New York.

Logg, A., Wells, G.N., 2010. DOLFIN: Automated finite element computing. ACM Trans. Math. Software 37 (2), http://dx.doi.org/10.1145/1731022.1731030.

Milovanovic, P., Vuković, Z., Antonijevic, D., Djonic, D., Zivkovic, V., Djuric, M., 2017. Porotic paradox: distribution of cortical bone pore sizes at nano and micro-levels in healthy vs. fragile human bone. J. Mater. Sci. Mater. Med. 28, 71. http://dx.doi.org/10.1007/s10856-017-5878-7.

Minonzio, J.-G., Bochud, N., Vallet, Q., Ramiandrisoa, D., Etcheto, A., Briot, K., Kolta, S., Roux, C., Laugier, P., 2019. Ultrasound-based estimates of cortical bone thickness and porosity are associated with nontraumatic fractures in post-menopausal women: A pilot study. J. Bone Miner. Res. 34 (9), 1585–1596. http://dx.doi.org/10.1002/jbmr.3733.

Minonzio, J.-G., Han, C., Cassereau, D., Grimal, Q., 2021. *In vivo* pulse-echo measurement of apparent broadband attenuation and Q factor in cortical bone: A preliminary study. Phys. Med. Biol. 66 (15), 155002. http://dx.doi.org/10.1088/1361-6560/ac1022.

Nguyen, S.-T., Vu, M.-B., Vu, M.-N., To, Q.-D., 2018. A homogenization approach for the effective drained viscoelastic properties of 2D porous media and an application for cortical bone. J. Mech. Behav. Biomed. Mater. 78, 134–142. http://dx.doi.org/10.1016/j.jmbbm.2017.11.020.

Núñez, J., Goring, A., Hesse, E., Thurner, P., Schneider, P., Clarkin, C., 2017. Simultaneous visualisation of calcified bone microstructure and intracortical vasculature using synchrotron X-ray phase contrast-enhanced tomography. Sci. Rep. 7, 13289. http://dx.doi.org/10.1038/s41598-017-13632-5.

O'Donnell, M., Jaynes, E.T., Miller, J.G., 1981. Kramers–Kronig relationship between ultrasonic attenuation and phase velocity. J. Acoust. Soc. Am. 69 (3), 696–701. http://dx.doi.org/10.1121/1.385566.

Panasenko, G.P., 2005. Multi-Scale Modelling for Structures and Composites. Springer, Dordrecht, Netherlands Norwell, MA.

Parnell, W., Abrahams, I., 2008. Homogenization for wave propagation in periodic fibre-reinforced media with complex microstructure. I—Theory. J. Mech. Phys. Solids 56 (7), 2521–2540. http://dx.doi.org/10.1016/j.jmps.2008.02.003.

Parnell, W.J., Grimal, Q., 2009. The influence of mesoscale porosity on cortical bone anisotropy. investigations via asymptotic homogenization. J. R. Soc. Interface 6 (30), 97–109. http://dx.doi.org/10.1098/rsif.2008.0255.

Parnell, W., Vu, M.B., Grimal, Q., Naili, S., 2012. Analytical methods to determine the effective mesoscopic and macroscopic elastic properties of cortical bone. Biomech. Model. Mechanobiol. 11, 883–901. http://dx.doi.org/10.1007/s10237-011-0359-2.

Penta, R., Gerisch, A., 2015. Investigation of the potential of asymptotic homogenization for elastic composites via a three-dimensional computational study. Comput. Vis. Sci. 17, 185–201. http://dx.doi.org/10.1007/s00791-015-0257-8.

Ramírez-Torres, A., Penta, R., Rodríguez-Ramos, R., Merodio, J., Sabina, F.J., Bravo-Castillero, J., Guinovart-Díaz, R., Preziosi, L., Grillo, A., 2018. Three scales asymptotic homogenization and its application to layered hierarchical hard tissues. Int. J. Solids Struct. 130–131, 190–198. http://dx.doi.org/10.1016/j.ijsolstr.2017.09.035.

Salguero, L., Saadat, F., Sevostianov, I., 2014. Micromechanical modeling of elastic properties of cortical bone accounting for anisotropy of dense tissue. J. Biomech. 47 (13), 3279–3287. http://dx.doi.org/10.1016/j.jbiomech.2014.08.019.

Sandrakov, G.V., 1999. Homogenization of elasticity equations with contrasting coefficients. Sbornik: Math. 190, 1749–1806. http://dx.doi.org/10.1070/SM1999v190n12ABEH000443.

Sasso, M., Haïat, G., Yamato, Y., Naili, S., Matsukawa, M., 2008. Dependence of ultrasonic attenuation on bone mass and microstructure in bovine cortical bone. J. Biomech. 41 (2), 347–355. http://dx.doi.org/10.1016/j.jbiomech.2007.09.001.

Sundh, D., Nilsson, A., Nilsson, M., Johansson, L., Mellström, D., Lorentzon, M., 2017. Increased cortical porosity in women with hip fracture. J. Int. Med. 281, 496–506. http://dx.doi.org/10.1111/joim.12587.

Szabo, T.L., 1995. Causal theories and data for acoustic attenuation obeying a frequency power law. J. Acoust. Soc. Am. 97 (1), 14–24. http://dx.doi.org/10.1121/1.412332.

Vennin, S., Desyatova, A., Turner, J., Watson, P., Lappe, J., Recker, R., Akhter, M., 2017. Intrinsic material property differences in bone tissue from patients suffering low-trauma osteoporotic fractures, compared to matched non-fracturing women. Bone 97, 233–242. http://dx.doi.org/10.1016/j.bone.2017.01.031.

Wu, Z., Ovaert, T., Niebur, G., 2012. Viscoelastic properties of human cortical bone tissue depend on gender and elastic modulus. J. Orthop. Res. 30, 693–699. http://dx.doi.org/10.1002/jor.22001.

Yamashita, J., Furman, B.R., Rawls, H.R., Wang, X., Agrawal, C.M., 2001. The use of dynamic mechanical analysis to assess the viscoelastic properties of human cortical bone. J. Biomed. Mater. Res. 58 (1), 47–53. http://dx.doi.org/10.1002/1097-4636(2001)58:1<47::AID-JBM70>3.0.CO;2-U.

Yi, Y.-M., Park, S.-H., Youn, S.-K., 1998. Asymptotic homogenization of viscoelastic composites with periodic microstructures. Int. J. Solids Struct. 35 (17), 2039–2055. http://dx.doi.org/10.1016/S0020-7683(97)00166-2.

Yousefian, O., Karbalaeisadegh, Y., Muller, M., 2021. Frequency-dependent analysis of ultrasound apparent absorption coefficient in multiple scattering porous media: application to cortical bone. Phys. Med. Biol. 66, 035026. http://dx.doi.org/10.1088/1361-6560/abb934.

Zhou, J., Cui, Z., Sevostianov, I., 2020. Effect of saturation on the elastic properties and anisotropy of cortical bone. Internat. J. Engrg. Sci. 155, 103362. http://dx.doi.org/10.1016/j.ijengsci.2020.103362.